

Cite this as:

M.I. Muglali, A. Erbe, Y. Chen, C. Barth, P. Koelsch, M. Rohwerder: *Electrochimica Acta*, **90**, 17-26 (2013).

Final copy-edited version of the manuscript is available from:

<http://dx.doi.org/10.1016/j.electacta.2012.11.116>

Modulation of electrochemical hydrogen evolution rate by araliphatic thiol monolayers on gold

Mutlu I. Muglali^a, Andreas Erbe^{a,*}, Ying Chen^{a,b}, Christoph Barth^c,
Patrick Koelsch^{c,d}, Michael Rohwerder^{a,1,**}

^a*Max-Planck-Institut für Eisenforschung GmbH, Department of Interface Chemistry and Surface Engineering, Max-Planck-Str. 1, 40237 Düsseldorf, Germany*

^b*Center for Electrochemical Sciences, Ruhr-Universität Bochum, Universitätsstr. 150, 44780 Bochum, Germany*

^c*Institute of Toxicology and Genetics, Karlsruhe Institute of Technology, Postfach 3640, 76021 Karlsruhe, Germany*

^d*National ESCA and Surface Analysis Center for Biomedical Problems, Department of Bioengineering, University of Washington, Box 35170, Seattle, Washington 98195-1750, USA*

Abstract

Electroreductive desorption of a highly ordered self-assembled monolayer (SAM) formed by the araliphatic thiol (4-(4-(4-pyridyl)phenyl)phenyl)methanethiol leads to a concurrent rapid hydrogen evolution reaction (HER). The desorption process and resulting interfacial structure were investigated by voltammetric techniques, *in situ* spectroscopic ellipsometry, and *in situ* vibrational sum-frequency-generation (SFG) spectroscopy. Voltammetric experiments on SAM-modified electrodes exhibit extraordinarily high peak currents, which differ between Au(111) and polycrystalline Au substrates. Association of reductive desorption with HER is shown to be the origin of

*Corresponding author; Phone: +49 211 6792 890, Fax: +49 211 6792 218

**Corresponding author; Phone: +49 211 6792 914, Fax: +49 211 6792 218

Email addresses: a.erbe@mpie.de, aerbe@arcor.de (Andreas Erbe),
rohwerder@mpie.de (Michael Rohwerder)

¹ISE member.

the observed excess cathodic charges. The studied SAM preserves its two-dimensional order near Au surface throughout a fast voltammetric scan even when the vertex potential is set several hundred millivolt beyond the desorption potential. A model is developed for the explanation of the observed rapid HER involving ordering and pre-orientation of water present in the nanometer-sized reaction volume between desorbed SAM and the Au electrode, by the structurally extremely stable monolayer, leading to the observed catalysis of the HER.

Keywords: Reductive SAM desorption; Hydrogen evolution; Catalysis; Sum frequency generation spectroscopy; Spectroscopic ellipsometry

1. Introduction

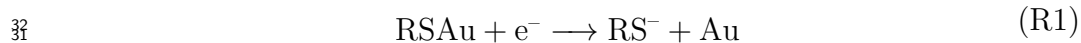
Self-assembled monolayers (SAMs) are often employed for electrochemical applications such as control of charge transfer [1, 2], production of (bio)electrochemical sensors [3–5], metal/organic/metal junctions [6–8], and barrier layers against metal corrosion [9–11]. It is essential to understand the effect of SAM-modified electrodes on electron transfer reactions, as well as their interfacial structure under electrochemical conditions for their ultimate use in electrolytic media.

In most cases, the rate of an interfacial chemical reaction is reduced by the presence of adsorbates because of their blocking of active sites on the surface, as has been shown, *e.g.*, for the oxygen reduction reaction (ORR) on Au(111) [9, 12, 13]. If the adsorbate blocks the active sites through covalent bonds, such a rate decrease is also expected for the HER. On the other hand, redox-active physisorbed monolayers have been shown to act as catalysts

15 towards the HER [14].

16 For thiol self-assembled monolayers (SAMs) on Au, HER occurs in an
17 electrode potential range beyond reductive desorption of the SAMs [15],
18 leading to a complex interplay between different interfacial reactions. To
19 understand this complex interplay, it is essential to understand the interfa-
20 cial properties of SAM-modified electrodes under electrochemical conditions.
21 In this context, the influence of the electrode potential on formation kinetics
22 [16, 17], structural properties [18–20], and ionic permeability of SAMs has
23 been subject to several works [19, 21]. Especially electrochemical desorp-
24 tion/readsorption studies revealed important details concerning the nature of
25 the interfacial interactions between a chemisorbed monolayer and a metallic
26 substrate, besides defining the applicable potential range for SAM-modified
27 electrodes.

28 On the cathodic side, this potential range is typically limited by the re-
29 ductive desorption of thiol-SAMs from the Au substrate, which is commonly
30 described by the simple reaction [22]



33 Although the cleavage of the Au-S covalent bond has been established, many
34 aspects of the entire electroreductive desorption mechanism of thiol mono-
35 layers are unclear and have been subject of a number of studies, in most
36 cases excluding the effect on and the role of the HER [23–37]. Besides the
37 currents originating from the Faradaic 1, incidental capacitive currents have
38 been reported during desorption of a SAM as a consequence of the transition
39 between a SAM-covered and a bare interface. Cathodic peaks originating
40 from capacitive currents are usually not larger than 20-30 % of the des-

41 orption currents, as reported for long-chain aliphatic thiols [23–25, 32–36],
42 because charges transferred during such capacitive processes are smaller than
43 the charges transferred during Faradaic reactions.

44 The state of the molecular units of SAMs during and after electrore-
45 ductive desorption is decisive for the electrode’s activity towards interfacial
46 reactions, including HER. After electroreductive cleavage of the S-Au bonds,
47 soluble molecules diffuse into the electrolyte, while long-chain alkanethio-
48 lates reside in the double layer region as a consequence of their poor water
49 solubility.[38] Within the double layer, chemically desorbed long-chain alka-
50 nethiolates form aggregates, as concluded from spectroscopic and microscopic
51 studies [26, 28, 30, 31]. Depletion of these aggregates has been proposed as
52 the source of additional capacitive currents, which are usually observed as
53 a separate peak in voltammograms during desorption of long *n*-alkanethiols.
54 This hypothesis was later disproven by a second-harmonic-generation study
55 [37]. In addition, vibrational sum-frequency-generation (SFG) spectroscopy
56 has been applied to investigate molecular ordering and orientation within
57 self-assembled monolayers at electrified interfaces [39–42], and *ex situ* af-
58 ter treatment at different potentials [38]. The majority of previous studies
59 of electroreductive desorption focused on commonly used aliphatic SAMs.
60 In recent years, interest has shifted towards SAMs consisting of aromatic
61 molecular units, due to their enhanced stability and interesting electric and
62 electronic properties [1, 2, 43–45]. So far, to the author’s knowledge, no de-
63 tailed desorption study of such technologically promising SAMs composed of
64 large aromatic molecules with more than two aromatic rings has been car-
65 ried out. Different in mechanism from multiwave desorption peaks observed

66 for *n*-alkanethiols, long araliphatic thiols show an extraordinary multiwave
67 response during electroreductive desorption [46]. The corresponding trans-
68 ferred charges are too large for a capacitive process and even larger than the
69 Faradaic desorption reaction. The magnitude of the unknown, desorption-
70 related Faradaic process points to involvement of the HER [46]. A full in-
71 vestigation of the physical state of the desorbed molecules on the electrode
72 surface requires spectroscopic or microscopy techniques combined with elec-
73 trochemistry.

74 This work examines the unusual desorption behavior of the highly ordered
75 araliphatic thiol monolayers using previously characterized SAMs of (4-(4-
76 (4 pyridyl)phenyl)phenyl)methanethiol (PyPP1) and 2-(4-(4-(4-pyridyl)phe-
77 nyl)phenyl)ethanethiol (PyPP2). A series of voltammetric measurements
78 have been performed to determine the origin of the extraordinarily large
79 cathodic peaks that appear after reductive desorption. Transient states at the
80 SAM-Au interface and within the monolayer film and during HER have been
81 monitored *in situ* and *in operando* by femtosecond-based broadband SFG
82 spectroscopy and spectroscopic ellipsometry. Combining the voltammetric
83 and spectroscopic results, a model is proposed explaining the voltammetric
84 response of electroreductive desorption of the investigated SAMs.

85 **2. Experimental**

86 *2.1. Samples*

87 PyPP1 and PyPP2 organothiols were synthesized as described elsewhere
88 [47]. Au(111) substrates were prepared by evaporating gold onto freshly
89 cleaved mica sheets at a substrate temperature of 450°C in a Leybold Uni-

90 vex 450 system. Prior to use, the Au films were annealed in a H₂ flame.
91 Polycrystalline Au (poly-Au) substrates were mechanically polished. SAMs
92 were formed by immersion of the Au substrates into 20 μM ethanolic thiol
93 solutions for 12-15 h. After removal from solution, samples were thoroughly
94 rinsed with ethanol and purged with nitrogen gas. All chemicals used were
95 in reagent grade.

96 2.2. Voltammetry

97 For all electrochemical measurements a Compactstat potentiostat (Ivium
98 Technologies, The Netherlands) was employed. Deaerated 0.1 M NaOH so-
99 lution was used as electrolyte. Cyclic voltammograms (CVs) on SAM-
100 modified Au(111) electrodes were measured with a scan rate of 50 mV s⁻¹,
101 unless stated otherwise. All electrode potentials E herein are referred to an
102 Ag/AgCl (3 M KCl) reference electrode. For determination of the charges Q
103 per electrode area transferred during a voltammetric peak, a linear baseline
104 was set between the vertices of the peaks in the curves of the current densities
105 j . This baseline was subsequently subtracted from the original j .

106 For hydrodynamic measurements a rotating disk electrode (RDE) assem-
107 bly, and a rotating ring-disk electrode (RRDE) assembly (Pine Research
108 Instruments, USA) were used. In both configurations, disk electrodes con-
109 sisted of a mirror polished polycrystalline Au disk. In the RRDE tip, around
110 the poly-Au disk (diameter 5 mm), a Pt ring was placed with 6.5 mm and 7.5
111 mm inner and outer diameters, respectively. Prior to measurements, both
112 the ring and the disk electrodes were modified with a PyPP1 monolayer, so
113 that during the measurement, thiolate adsorption on the ring was prevented.
114 In this way, any oxidative current detected on the ring could directly be

115 assigned to H₂ oxidation at the applied ring potential ($E_R = -0.5$ V) but
 116 not to oxidative adsorption of thiolates. Collection efficiency of the SAM-
 117 modified Pt ring was determined to be ≈ 0.05 (compared to 0.43 without
 118 SAM modification).

119 2.3. Ellipsometry

120 For spectroscopic ellipsometry measurements, a PyPP1/Au(111) (2 cm x
 121 1.5 cm) sample was placed in a homemade PTFE electrochemical cell with
 122 suitable apertures for incident and reflected light, as well as for a Ag/AgCl
 123 (3 M KCl) microreference electrode and a Pt spiral as counter electrode.
 124 The cell was placed in the beam path of a SE 800 spectroscopic ellipsometer
 125 (Sentech Instruments, Germany) [48, 49]. The ellipsometric angles Ψ and Δ
 126 were measured every ≈ 5 s for wavelengths λ from 300 to 820 nm during CV
 127 measurements with a scan rate of 5 mV s⁻¹ between 0 V and -1.6 V. The
 128 angles are transformed into the ellipsometric ratio $\rho = \frac{r_p}{r_s} = \tan(\Psi) e^{i\Delta}$ with
 129 $i = \sqrt{-1}$. [50]

The ratio of the amplitude reflection coefficients r_p and r_s for p- and s-
 polarized light, respectively, was analyzed using a perturbation approach [51].
 The perturbation parameter J_1 is related to the transition of the dielectric
 function $\epsilon_s(z)$ of the interfacial region perpendicular to the interface in z -
 direction,

$$J_1 = \int_{-\infty}^{+\infty} \frac{(\epsilon_1 - \epsilon_s(z))(\epsilon_s(z) - \epsilon_2)}{\epsilon_s(z)} dz. \quad (1)$$

For layer and layer systems with a total thickness small compared to the λ ,
 ρ is expanded to first order around a step profile in the dielectric function

with ρ_0 , yielding [51]

$$\rho = \rho_0 - \frac{2iq_1K^2}{r_s^{(0)}\epsilon_1^2\epsilon_2(q_1/\epsilon_1 + q_2/\epsilon_2)^2}J_1, \quad (2)$$

where

$$r_s^{(0)} = \frac{(q_1 - q_2)}{(q_1 + q_2)} \quad (3)$$

Here,

$$K = \frac{2\pi\sqrt{\epsilon_1}}{\lambda} \sin(\theta_1) \quad (4)$$

is the wavevector component parallel to the interface at which a plane wave impinges under an angle of θ_1 , while

$$q_k = \frac{2\pi\sqrt{\epsilon_k}}{\lambda} \cos(\theta_k), k \in 1, 2 \quad (5)$$

130 is the wavevector component perpendicular to the interface in the respective
 131 medium, where index 1 indicates the medium of incidence and 2 indicates
 132 the gold substrate. Literature values have been used for the wavelength-
 133 dependence of the dielectric functions ϵ_1 and ϵ_2 of the electrolyte [52], and
 134 gold substrate [53, 54], respectively. Eq. 2 can be solved for J_1 and used for
 135 a computation of J_1 from experimental data.

136 For measurements of ρ_0 , E of a bare Au electrode in 0.1 M NaOH was
 137 varied between 0 and -0.5 V. In this range, recorded changes were on the
 138 order of the noise level.

139 2.4. Sum-Frequency-Generation Spectroscopy (SFG)

The SFG measurements were performed on a home-built SFG spectrom-
 eter [55]. Briefly, an etalon-shaped narrowband visible laser beam with
 frequency ω_{VIS} fixed at 800 nm and a tunable broadband (100 fs pulse

duration) infrared (IR) laser beam are spatially and temporally superimposed at the sample/electrolyte interface. Superposition results in the generation of a third beam at the sum-frequency of the two incident beams $\omega_{\text{SFG}} = \omega_{\text{VIS}} + \omega_{\text{IR}}$. The resulting SFG intensity is

$$N_{\text{SFG}} \propto |\chi^{(2)}|^2 N_{\text{IR}} N_{\text{VIS}} \quad (6)$$

with

$$\chi^{(2)} = \chi_{\text{NR}}^{(2)} + \chi_{\text{R}}^{(2)} = \chi_{\text{NR}}^{(2)} + \sum_k \left| \frac{A_k}{(\omega_{\text{IR}} - \omega_k) + i\gamma_k} \right| e^{i\phi_k}, \quad (7)$$

140 where $\chi_{\text{NR}}^{(2)}$ is the second-order susceptibility of the metallic substrate. The
 141 resonant contribution of the second-order susceptibility $\chi_{\text{R}}^{(2)}$, which in this
 142 case originates exclusively from the SAM, is the superposition of a number
 143 of resonances, each with an amplitude A_k , frequency ω_k and the phase dif-
 144 ference ϕ_k between substrate and resonant response. The damping constant
 145 of the k^{th} -vibration is denoted as γ_k . N_{VIS} and N_{IR} are the intensities of the
 146 two incident beams. The non-resonant background consisting of contribu-
 147 tions $\chi_{\text{NR}}^{(2)}$ of the Au substrate were suppressed by delaying visible and IR
 148 laser pulses by 400 fs [56]. The effects of SAM desorption were finally mon-
 149 itored by centering the IR beam to 1600 cm^{-1} and recording spectra under
 150 dry air conditions using a purge-box [55]. All spectra were recorded in p
 151 polarizations for all beams (SFG, VIS, and IR). Incident angles for the IR
 152 and VIS beams were adjusted to 55° and 60° , respectively.

153 In order to perform SFG measurements under E -control in electrochem-
 154 ical media, a thin-layer analysis cell [55] was modified (Fig. 1) by building
 155 electrolyte (0.1 M NaOH) reservoirs at the sides of the CaF_2 prism using a
 156 chemically resistive two-component adhesive (X60, HBM Inc., USA). Two

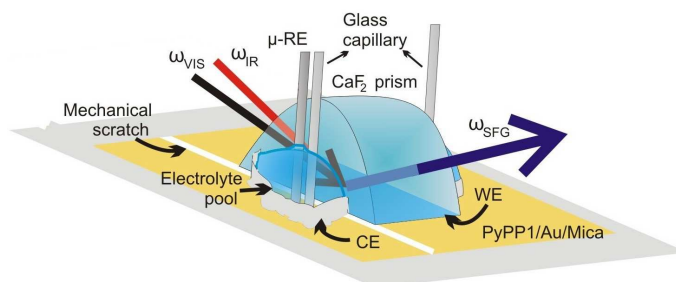


Figure 1: Sketch of the beam path and the arrangement of the electrodes in the modified thin-layer analysis cell for SFG measurements. The reflected VIS and IR beams are not displayed.

157 glass capillaries containing a part of the electrolyte solution were dipped into
 158 each of the electrolyte pools and slowly released electrolyte into the reser-
 159 voir during the measurements in order to compensate evaporation in dry air
 160 conditions. PyPP x /Au/Mica substrates underlying the prism were extended
 161 over the larger side of the prism into the reservoir. Au films on the substrates
 162 were separated into two parts at the boundary between the prism and reser-
 163 voir by a mechanical scratch so that the part underneath the prism served as
 164 working electrode (WE) and the other part within the reservoir as counter
 165 electrode (CE). An Ag/AgCl (3 M KCl) microreference electrode (RE) was
 166 placed next to the prism in order to minimize the potential drops. In this
 167 configuration, the area exposed to the incident beams was approximately 0.5
 168 cm away from the reference and counter electrodes. The thickness of the
 169 electrolyte layer underneath the CaF₂ was estimated to be <1 μm, which
 170 enabled homogenous potential control over the entire sample surface. Right
 171 after the assembly of the electrochemical SFG cell, a series of spectra with an
 172 exposure time of 0.4 s in the background-suppressed mode was started. Af-

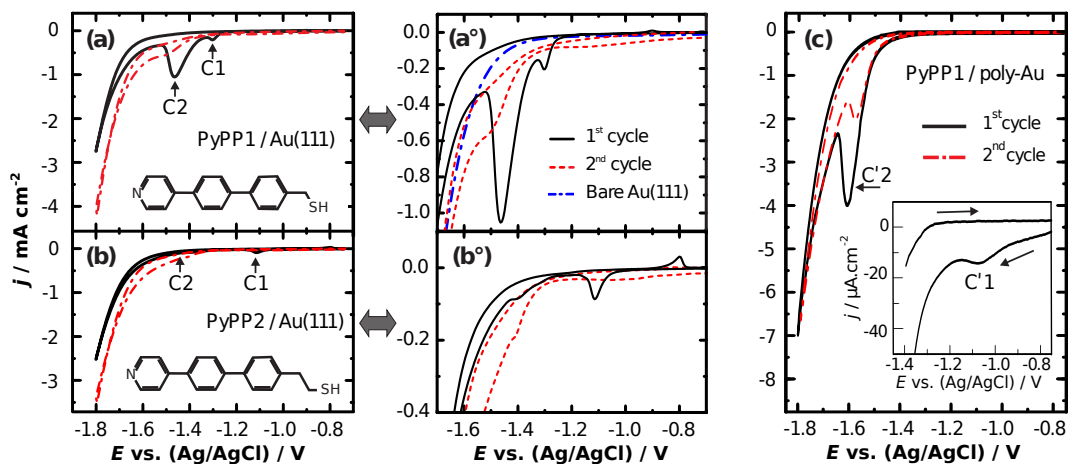


Figure 2: First and second CV scan cycles obtained from (a) PyPP1-modified Au(111) and (b) PyPP2-modified Au(111). In (a) a voltammogram of bare Au(111) is also given (dashed line). (a°) and (b°) show an enlarged view around the cathodic and anodic peaks of (a) and (b), respectively. (c) PyPP1-modified poly-Au in 0.1 M NaOH. The inset shows the zoom of the low-current region of the first cycle. Subsequent scans yielded similar peaks but with smaller intensities as a result of partial readsorption of thiolates.

173 ter 10 recorded spectra at the open circuit potential (OCP), the potentiostat
 174 was switched on performing a CV starting from the first vertex at 0 V to the
 175 second vertex at -1.6 V with a scan rate of 50 mV s^{-1} . The SFG signal was
 176 then continuously recorded for 10 CV cycles. For obtaining a quantitative
 177 measure of the SFG signal, the recorded background-suppressed spectra were
 178 integrated without any further data treatment.

179 3. Results and Discussion

180 3.1. Cyclic Voltammetry (CV)

181 Fig. 2 presents the CVs obtained for the SAM-modified Au electrodes in
 182 0.1 M NaOH and compares them to the curve for pure Au(111). Adsorption

183 sites on an Au(111) surface differ for PyPP1 and PyPP2 because of differ-
184 ent molecular tilt angles arising from the “odd-even” effect involving the
185 methylene spacers [57]. PyPP1 adsorbs on Au(111) with a $(2\sqrt{3} \times \sqrt{3})R30^\circ$
186 overlayer structure, whereas PyPP2 yields a $(5\sqrt{3} \times \sqrt{3})\text{rect}$ structure on the
187 same substrate [57]. The 25% lower surface coverage of PyPP2 on the surface
188 results in weaker intermolecular interactions compared to PyPP1 [46, 57].
189 Hence, desorption potentials (C1 peaks in the CVs) of the dilute PyPP2
190 SAM and the compact PyPP1 SAM differ accordingly. Although C1 peak
191 potentials vary between PyPP1- and PyPP2-modified Au(111) electrodes,
192 both systems yield double peaks within the electroreductive desorption re-
193 gions, as shown in Fig. 2a and b, respectively. For the PyPP1/Au(111)
194 electrode, the C1 peak at -1.30 V is followed by a much larger second peak
195 C2 at -1.47 V. By integration of these peaks, $Q \sim -0.06 \text{ mC cm}^{-2}$ for C1
196 and -1.32 mC cm^{-2} for C2. For desorption of a PyPP1 SAM with the given
197 overlayer structure on Au(111), a total Faradaic charge of $\sim -0.06 \text{ mC cm}^{-2}$
198 is expected according to Faraday’s Law for a single electron transfer process,
199 $\Gamma = Q/F$, where Γ is the surface coverage, and F is the Faraday constant.
200 The experimental results show the major portion of the theoretically esti-
201 mated charge for desorption of a complete monolayer to be reached during
202 the C1 peak. Remarkably, the integrated current of the C2 peak corresponds
203 to a 22-times larger reductive charge, which results obviously from a Faradaic
204 process other than thiol desorption. The peak current, hence also the reac-
205 tion rate, in this second cathodic peak is ~ 10 times higher than the current
206 at the same potential on bare Au(111) during the first cycle, and is still ~ 3
207 times as high as bare Au(111) during the second cycle. In the voltammogram

208 of the PyPP2/Au(111) electrode, the C1 peak at -1.11 V yields $Q \sim -0.06$ mC
209 cm^{-2} , similar to PyPP1/Au(111). Subsequently, a much less pronounced C2
210 peak appears at -1.42 V with $Q \sim -0.01$ mC cm^{-2} . A direct relationship be-
211 tween monolayer structure and the rate of the concomitant Faradaic reaction
212 is reflected in the CVs of compact PyPP1 and non-compact PyPP2 SAMs on
213 Au(111). According to a model, compact monolayers such as PyPP1 desorb
214 *via* a homogeneous reduction process all over the electrode surface, whereas
215 etching centers are created in more permeable monolayers and desorption
216 propagates successively at the edges of these etching centers [58, 59]. The
217 lower ionic permeability expected for PyPP1 is supposed to cause slower dif-
218 fusion of counter ions (here Na^+) from the electrolyte to the sulfur heads
219 through the thiols, consequently shifting the desorption potential to more
220 negative values [46].

221 The observed extraordinary voltammetric response upon the electrore-
222 ductive desorption of PyPP1 SAMs becomes even more striking when the
223 monolayer is adsorbed on a poly-Au surface instead of Au(111). For the
224 PyPP1/poly-Au electrode, again a double peak is observed in the voltam-
225 mogram (Fig. 2c). However, the C'1 peak is barely visible next to the massive
226 C'2 peak. (Here, the peaks are designated as C'1 and C'2 to stress the slight
227 differences in origin of the peaks.) A $Q \sim -0.01$ mC cm^{-2} for the first peak
228 at -1.15 V suggests that in this peak, only a small portion of the monolayer
229 desorbs, which most likely consists of weakly bound thiols, *e.g.* at domain
230 boundaries. The residual major portion of the monolayer desorbs at more
231 negative potentials in the dominant second peak at -1.61 V. Integration yields
232 $Q \sim -2.30$ mC cm^{-2} for C'2. Obviously, on a poly-Au substrate, the PyPP1

233 SAM desorbs at more cathodic potentials compared to an Au(111) substrate.
234 At the same time, larger reductive currents are observed. The negative po-
235 tential shift for desorption of the monolayer on a poly-Au substrate compared
236 to Au(111) can be explained by the increased electrochemical stability of the
237 monolayer on the polycrystalline surface. It is well-known that the energy
238 required to desorb SAMs from a gold surface is minimum for Au(111) [60–
239 63]. Assuming that the poly-Au substrate has a considerable proportion of
240 low index surfaces other than (111), desorption at more negative potentials
241 is quite reasonable. However, it is astonishing that by using a poly-Au sub-
242 strate, the additional Faradic reaction overlaps with the desorption reaction,
243 yielding a 75% larger Q compared to the PyPP1/Au(111) electrode.

244 Further CV measurements at different scan rates (not shown, see also
245 Section 3.3) indicate that the C2/C'2 peak is related to a diffusion-controlled
246 reaction at the corresponding peak potential. On the other hand, the area
247 under the C1/C'1 peak (i.e. the charges) is almost independent of the scan
248 rate, as expected for a peak purely related to desorption.

249 The CV results show that the main body of the monolayer desorbs from
250 a poly-Au substrate within the range of the C'2 peak. However, for the
251 PyPP1/Au(111) system, both peaks are large enough to contain desorption
252 currents of a monolayer so that the origins of the corresponding peak cur-
253 rents cannot be distinguished. For determining the beginning and the end
254 of the monolayer desorption process on this system, changes at the elec-
255 trolyte/PyPP1/Au interface during a CV scan were tracked using ellipsom-
256 etry.

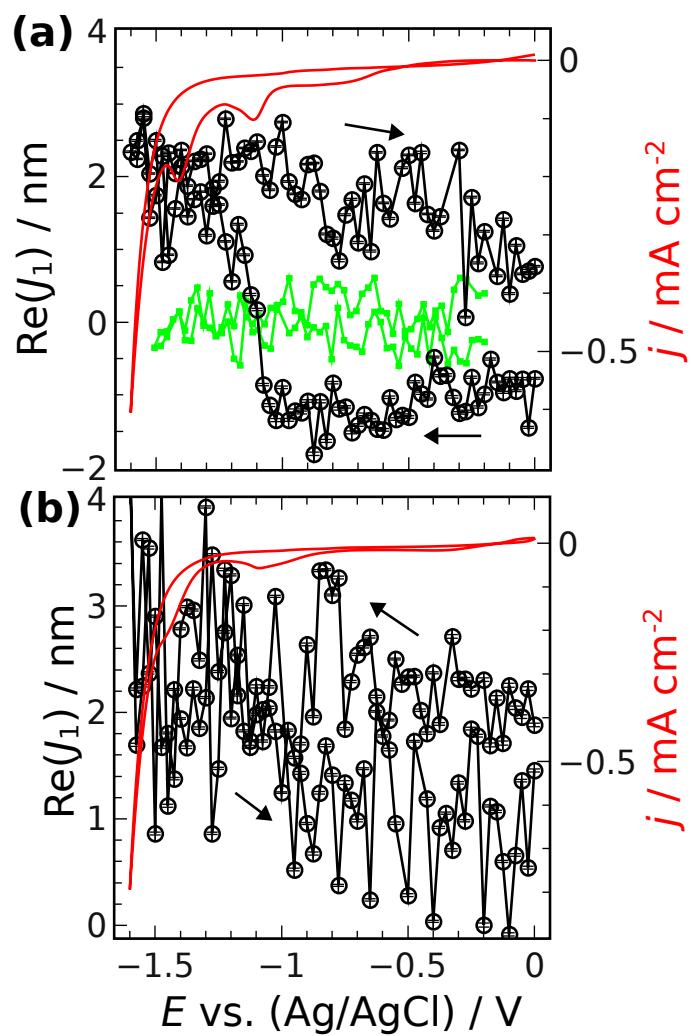


Figure 3: Real part of J_1 averaged from 340-360 nm (\circ , scale on the left, see text for rationale of wavelength range) during (a) the first and (b) the second CV scan ($-$, scale on the right) of PyPP1/Au(111) in 0.1 M NaOH. (a) includes $\text{Re}(J_1)$ ($-$) on Au(111) without SAM. Arrows indicate the respective potential scan direction. Scan rate: 5 mV s⁻¹.

257 *3.2. Ellipsometry*

258 Fig. 3a shows the real part of J_1 as function of E during the first CV scan
259 of a freshly prepared PyPP1/Au(111) sample. Different from the previously
260 presented CV measurement (Fig. 2a), in this experiment the scan rate was set
261 to 5 mV s^{-1} for achieving a good synchrony between the applied potentials
262 and ellipsometric data acquisition. A significant decrease is observed in the
263 current of the second peak compared to the preceding first peak at this low
264 scan rate.

265 Taking a look at the corresponding ellipsometry data, a stable and con-
266 stant $\text{Re}(J_1)$ is observed until the onset of the C1 peak. The magnitude
267 observed of $\text{Re}(J_1) \sim -1 \text{ nm}$ in the given wavelength range is expected for
268 an organic layer of a thickness of $\sim 1.5 \text{ nm}$, consistent with an intact SAM.
269 The wavelength-dependence of the data is mainly given by the wavelength-
270 dependence of ϵ_2 , which means that the curves appear similar in shape but
271 different in magnitude at all wavelengths. The wavelength range displayed
272 here was chosen as it is the region where ϵ_2 is closest to 0, which simplifies the
273 analysis according to Eq. 1. At the onset of the C1 peak in the CV, $\text{Re}(J_1)$
274 increases and reaches zero approximately in the middle of the desorption
275 peak. $\text{Re}(J_1) = 0$ corresponds to a complete absence of a layer, or the can-
276 cellation in Eq. 1 of the effect of regions with positive or negative dielectric
277 constant contrast. $\text{Re}(J_1)$ continues to rise above zero until the onset of the
278 C2 peak, and remains constant with further increasing cathodic potentials
279 until the potential vertex at -1.6 V . The positive value of $\text{Re}(J_1)$ implies that
280 the dominating layer in the interfacial refractive index profile now has a real
281 part of the dielectric constant at the respective frequency between the value

282 of the electrolyte (~ 1.8) and Au (~ -1.1), which is untypical for organic mate-
283 rials. During the reverse scan, re-adsorption is observed as a slight decrease
284 in $\text{Re}(J_1)$, which remains at values > 0 . Readsorption is barely visible in the
285 CV current, because the scan rate is not high enough to display respective
286 charges. The results obtained during the subsequent second scan are shown
287 in Fig. 3b. In the direction of increasing cathodic potential, $\text{Re}(J_1)$ resembles
288 closely the backward scan of Fig. 3a. Desorption is barely visible in $\text{Re}(J_1)$,
289 but it is in the CV. In the backward scan, values of $\text{Re}(J_1)$ approach more
290 and more the value of 0. The increased fluctuations in $\text{Re}(J_1)$ in the later
291 stages of the experiment are attributed to the presence of H_2 bubbles, which
292 remain on the surface after E is entering the regime of HER for the first time,
293 and the consequent increase in scattered light intensity on the expense of the
294 detected reflected intensity. It must be pointed out that the changes in the
295 curves between the different scans are not due to drift of the instrument, but
296 are caused by genuine changes in the interfacial structure. Corresponding
297 experiments with bare Au show highly repeatable scans.

298 The presented ellipsometry results reveal information about the state
299 of the PyPP1/Au interface during electrochemical polarization. The main
300 change in $\text{Re}(J_1)$ is observed during the first forward CV scan between the
301 C1 and C2 peaks. In this potential regime, desorption of the SAM occurs,
302 however, its constituents remain present near the interface. During subse-
303 quent readsorption, $\text{Re}(J_1)$ is still far away from its initial value and even
304 shows opposite sign to the initial value. One might expect that the SAM
305 loses all order during the desorption process, but SFG measurements, which
306 will be discussed later, show that order is maintained in the course of des-

307 orption, and is also maintained over at least 10 CV cycles. The most likely
308 explanation for the large effect in the first scan compared to all other is that
309 desorption leads to the presence of a layer or patches of low refractive index
310 between SAM and Au surface or between SAM and electrolyte. The value of
311 $\text{Re}(J_1) \sim 2$ nm after the desorption can be explained by the presence of an
312 effectively ~ 2.6 nm thick layer of a material with $\epsilon_s = 1$, if a total loss of the
313 SAM is assumed. As the SAM is still present, the effective layer thickness
314 must be even higher. The presence of macroscopic H_2 bubbles, which are
315 visible below -1.4 V, cannot account for the observed effect. Macroscopic
316 bubbles barely affect $\text{Re}(J_1)$, as has been confirmed in control experiments
317 in the absence of a SAM. Results from one control experiment are shown in
318 Fig. 3a. The aforementioned layer of low refractive index is likely in part
319 to be consisting of adsorbed H_2 , which starts to form below the desorption
320 potential. As not all gas is removed from the system when scanning in an-
321 odic direction, it may remain adsorbed, explaining the large and irreversible
322 shift to positive values of $\text{Re}(J_1)$. Further, desorption may also lead to sub-
323 stantial changes in the electronic structure of the Au surface, resulting in
324 respective irreversible changes of the dielectric function of Au near the inter-
325 face. A third possibility is a substantial change in solvent structure around
326 the desorbed SAM. This last explanation is, however, unlikely, because even
327 relatively large changes result only in rather weak effects on the dielectric
328 constant at optical frequencies.

329 It is also worth to underline an important result from the comparison of
330 the ellipsometric and CV results. The intensities of the two voltammetric
331 peaks and the degree of shift in $\text{Re}(J_1)$ do not match. This observation

332 indicates different mechanisms as the sources of the two subsequent cathodic
333 peaks on the voltammograms of PyPP1/Au(111) samples. Consequently, the
334 first reductive peak can be assigned mainly to the desorption of the SAM.
335 In order to elucidate the origin of the large excess currents appearing as the
336 second peak on PyPP1/Au(111) and overlap with the desorption currents
337 inside the same peak on PyPP1/poly-Au systems, further investigations were
338 done by hydrodynamic voltammetric measurements.

339 *3.3. Hydrodynamic voltammetry*

340 So far, the observed excess cathodic charges were postulated to result
341 mainly from a parallel Faradaic reaction concomitant to desorption of a
342 PyPP1 monolayer. HER is a likely candidate as the possible source of the
343 generated currents, because these excess currents are observed at potentials
344 where HER is thermodynamically possible [46]. In order to confirm the role
345 of H₂, RRDE measurements were performed using a PyPP1/poly-Au disk
346 electrode surrounded by a Pt ring, which was also modified with PyPP1
347 monolayer without extermination of the H₂ sensitivity. Fig. 4 shows the
348 voltammograms for the ring and disk electrodes at 900 RPM angular rotation
349 speed in 0.1 M NaOH. Both the ring and the disk voltammograms look quite
350 symmetrical. Similar to the CV shown in Fig. 2c, the PyPP1/poly-Au disk
351 electrode shows a desorption-related large cathodic peak covering a potential
352 range between -1.4 V and -1.7 V. On the ring electrode, a corresponding
353 oxidative peak is observed. After correction of the ring voltammogram re-
354 garding its collection efficiency, the absolute value of the charge underneath
355 the anodic peak on the ring corresponds to ~90% of the of the cathodic
356 peak charge on the disk voltammogram. The relation between the ring and

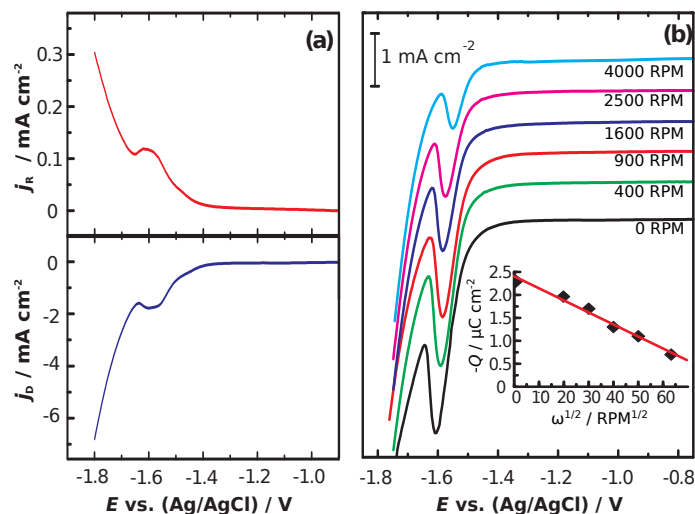


Figure 4: (a) RRDE data. Voltammograms obtained from PyPP1/poly-Au disk (j_D) and PyPP1/Pt ring (j_R) during the first scan cycle in 0.1 M NaOH with 900 RPM angular rotation speed and 50 mV s^{-1} scan rate. Ring potential was fixed at -0.5 V . (b) RDE data. Voltammograms of PyPP1/poly-Au electrode in 0.1 M NaOH at various angular rotation speeds ω . The inset shows the reductive charge density vs. $\sqrt{\omega}$.

357 disk currents is only approximate, because the determination of the collec-
 358 tion efficiency of a thiol modified ring is prone to errors. Nonetheless, since
 359 readsorption of released thiolates on the thiol modified ring can be ruled out,
 360 this anodic peak can be assigned mainly to oxidation of H_2 that is formed on
 361 the disk electrode concomitant to desorption of the monolayer. The observed
 362 C2 and C'2 peaks in the CVs can therefore be related to the evolution of H_2 .
 363 Because in this peak, the HER is significantly faster than on bare Au, the
 364 term “rapid HER” will be used here to described this special kind of HER.

365 In order to investigate the relationship between HER kinetics and SAM
 366 desorption, further hydrodynamic voltammetry experiments were carried
 367 out using identical PyPP1/poly-Au electrodes at varying electrode angu-

lar rotation speeds. A series of the hydrodynamic voltammograms for the PyPP1/poly-Au electrodes is presented in Fig. 4b. At each rotation speed the cathodic peak corresponding to C'2 is visible. However, the peak potential of the large peak gradually shifts to more anodic potentials with increasing rotation rates. Under hydrodynamic conditions, after cleavage of the S-Au bonds, thiolates are expected to diffuse faster away from the double layer region at high rotation speeds, as shown in previous experiments [64]. The transport of H₂ away from the electrode is also likely to contribute to transport of thiolates away from the electrode surface. At slower rotation, thiolates suspended in the double layer should slow down desorption of the remaining thiols [64]. Therefore, a SAM desorbs at slightly more anodic potentials when the electrode rotation speed is increased. For the investigated PyPP1/poly-Au electrodes, the total potential shift amounts to 60 mV (from -1.61 V to -1.55 V) between 0 and 4000 RPM. Due to the association between SAM desorption and rapid HER, the reductive peaks shift without changing their shape. Interestingly, peak charges decrease with increasing angular rotation speed (inset in Fig. 4b). These results indicate that retention time of the desorbed PyPP1 molecules has an influence on the HER kinetics. At this point, it becomes critical to know in what structural state the thiolates reside above the Au surface after desorption. The following experiment using vibrational SFG spectroscopy addresses this question.

3.4. SFG vibrational spectroscopy

For monitoring order of thiol/thiolate molecules during voltammetric scans, SFG spectroscopy was applied both *in situ* and in real time. Measurements were performed using Au(111) substrates, because flat surfaces are re-

393 quired to obtain adequate spectroscopic data. In addition to PyPP1/Au(111),
394 a PyPP2/Au(111) sample was investigated for comparison, which has a dif-
395 ferent structural quality and voltammetric response with less pronounced
396 additional Faradaic contributions, as shown in Fig. 2.

397 Fig. 5a shows the first one and a half voltammetric cycles of a typical
398 SFG experiment. The spectrum shows an SFG band attributed to the ring
399 vibration of the pyridine moiety of PyPP1, centered around 1600 cm^{-1} [57].
400 This mode was chosen because a measurement of the full SFG spectrum has
401 shown this band to be extremely intense. This extremely high intensity is
402 required for real-time measurements during the CVs. The evolution of the
403 signal intensity over time is alternating presumably due to nonlinear $\chi^{(3)}$
404 effects related to the coupling of visible, IR and static electric field at the
405 interface, which is discussed in detail elsewhere [65]. No further significant
406 change is observed in the intensity curve during the voltammetric scan, not
407 even in the peak potential regions below -1.25 V . This stable alternating sig-
408 nal indicates that the two-dimensional crystalline order of the monolayer is
409 persevered at all applied potentials. The SFG signal obtained from ordered
410 PyPP1 structures is not necessarily acquired only from the thiols directly
411 present on the Au(111) surface but also from the surface plane of the electri-
412 cal double layer. The first two CV scans recorded in parallel of SFG spectral
413 acquisition are shown in 5 b. The curves are slightly different compared to
414 those in Fig. 2, because of the different cell geometry. Especially the read-
415 sorption peak is more pronounced. Overall, CV data shows that after each
416 cycle, the amount of the readsorbed molecules becomes smaller. Hence the
417 observed stable SFG signals comprise contributions of both adsorbed and

418 suspended molecules as long as they remain ordered. In Fig. 5c the nor-
419 malized integrated SFG signals are plotted as function of the number of CV
420 cycles the electrode was subjected to. Because the intensity of the signal is
421 related to the order, number density, and orientation of molecules, a decrease
422 in the maximum intensity value indicates loss in the structural molecular ar-
423 rangement within the surface plane. Astonishingly, the signal obtained from
424 PyPP1 does not show significant variations after 10 voltammetric scan cy-
425 cles between 0 V and -1.6 V. On the other hand, the intensity for PyPP2
426 decreases continuously after each cycle. After 10 cycles, the PyPP2 signal
427 has almost vanished completely due to loss of order and/or decreased num-
428 ber density within the SAM. After leaving the PyPP1 monolayer at open
429 circuit for ~ 30 min after desorption experiments, the signal of PyPP1 has
430 also completely disappeared, indicating a diffusion of the molecules from the
431 surface into the bulk.

432 It is worth noting that readsorption peaks in the CVs of Section 3.1,
433 as well as those measured in the CVs during SFG experiments, are small,
434 considerably smaller than the desorption peaks. In a previous work, read-
435 sorption was quantified of PyPP1 and PyPP2 between -0.2 and -1.8 V [46]:
436 25 % of PyPP1 and ~ 50 % of PyPP2 readsorb after each cycle. However,
437 the molecules remain physisorbed to the electrode surface, even though the
438 Au-S bond is broken. SFG vibrational spectra do not distinguish between
439 ordered layers covalently bound to Au and ordered layers physisorbed to Au.
440 Therefore, the presence in the SFG spectra of the characteristic vibrational
441 mode from the molecules shows layer order, and hence also PyPP x presence,
442 in the interfacial region.

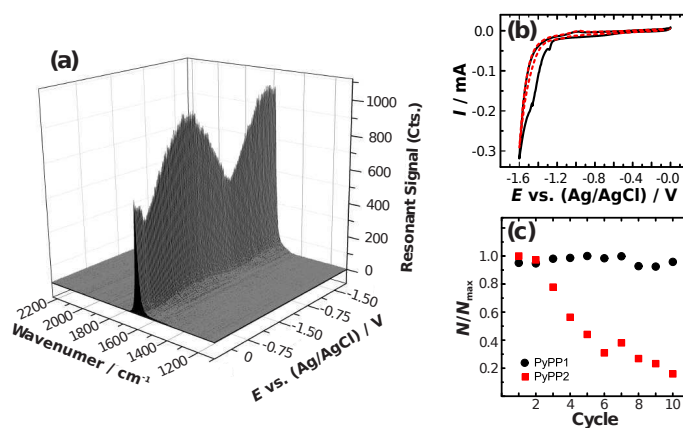


Figure 5: (a) Evolution of a pyridine ring vibration of PyPP1 on Au(111) during potential sweeps from 0 V to -1.6 V, back to 0 V, to finally -1.6 V, corresponding to one and a half CV cycles, as measured with SFG vibrational spectroscopy. (b) First two CV scans recorded in the SFG cell during acquisition of spectra shown in (a). (c) Integrated SFG intensity of the observed band from PyPP1/Au(111) and PyPP2/Au(111) during ten CV cycles. The integrated SFG signals are normalized to the maximum signal obtained from an ordered SAM for each thiol.

443 3.5. Discussion of rapid HER origin

444 The combination of the voltammetric and spectroscopic results obtained
445 from PyPP1 and PyPP2 modified Au samples reveals two important features
446 that make the desorption process especially of PyPP1 extraordinary com-
447 pared to the desorption of any aliphatic or short araliphatic thiol reported
448 to the author’s knowledge. The first extraordinary feature is the preserva-
449 tion of two-dimensional order of the reductively desorbed thiolates within
450 the double layer region, that exists over a long period of time and a large
451 potential range after desorption. The second feature is the association of
452 rapid HER with the desorption of the SAMs. These two features are closely
453 related, considering the observed differences in desorption between PyPP1
454 and PyPP2 SAMs. The correlation between these features helps to interpret
455 the complicated voltammetric desorption behavior on a solid ground.

456 Previous studies with aliphatic thiols showed that the structure of the
457 desorbed thiols undergoes a transition from upright molecular oriented films
458 to aggregates [26, 27, 29, 30, 66], or a striped phase with flat lying dithiol
459 molecules [67], in the electrochemical double layer region. Based on subtrac-
460 tively normalized interfacial infrared spectra [27, 66], and *in situ* scanning
461 tunneling microscopy studies [26], aggregates of long *n*-alkanethiolates have
462 been proposed to be in form of micelles. The micelle formation process
463 involves a competition between repulsive forces among negatively charged
464 sulfur head groups, attractive van der Waals forces among the chain units,
465 and hydrophobic forces. Hydrophobic termination groups accelerate micelle
466 formation. Taking all attractive and repulsive contributions into account, the
467 shape of the aggregates can be estimated from the semiempirical “packing

parameter” $v/(a_0l_c)$ involving the optimal surface area a_0 of the molecu-
lar head group, chain length l_c , and chain volume v [68]. For hydrocar-
bon amphiphiles, micelle formation becomes favorable if $v/(a_0l_c) < 1/3$ [68].
Due to the small $v/(a_0l_c)$ of the long aliphatic thiols with conformational
disorder in the desorbed state, micelle formation is conceivable for the n -
alkanethiolates. On the other hand, as the araliphatic chain is rather rigid,
araliphatic molecules exhibit a shape close to a cylinder, where $v/(a_0l_c) \sim 1$.
This value of $v/(a_0l_c)$ implies favorable formation of planar aggregate struc-
tures. Consequently, loss of crystalline order after reduction is expected to
occur slower for long araliphatic thiols. According to the SFG spectroscopy
measurements, for the thiolates of PyPP1 the crystalline structures inherited
from the chemisorbed monolayer are preserved in both voltammetric peak re-
gions (Fig. 5). According to the structural differences between PyPP1 and
PyPP2 monolayers, an even more stable ordered thiolate structure is ex-
pected for the compact PyPP1 SAM, which is confirmed by the presented
SFG results. These results are clear indication of the astonishingly long life-
time of the ordered thiolate structures for the investigated SAMs, especially
for PyPP1.

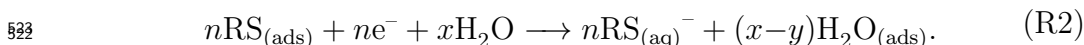
Apart from the stable structural order of the desorbed thiolates, a sec-
ond striking result is the detection of HER concomitantly to desorption of
the PyPP1 monolayer. On poly-Au, a rapid HER was found to occur si-
multaneously with the desorption of the main fraction of the SAM. On the
other hand, based on the ellipsometry results, these two reactions are not
simultaneous on Au(111) surfaces, where HER is found to occur only after
desorption of the SAM. Both processes are observed as separate peaks

493 in voltammograms (Fig. 3). The first reductive peak originates mainly from
494 SAM desorption, as confirmed by shift in $\text{Re}(J_1)$ at the corresponding po-
495 tentials. Because no pronounced shift in $\text{Re}(J_1)$ is detected in the potential
496 region of the subsequent large peak, it can be deduced that this peak consists
497 mainly of HER currents. When the rapid HER starts, the surface is already
498 saturated with H_2 , so the main fraction of the additionally produced H_2 is
499 leaving the system as gas, therefore it is not present in the interfacial region.
500 This finding can be generalized for the other members of the araliphatic thiol
501 series, including PyPP2, which also yields excess cathodic currents in parallel
502 to the thiol reduction process as observed on Au(111) surfaces.

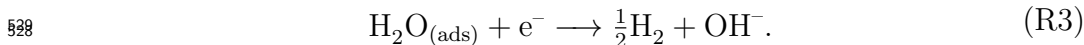
503 Considering the results of the RDE measurements, a relationship between
504 the rate of the HER (hence, catalytic activity of a surface towards HER) and
505 the thiolate's lifetime in the surface plane of the electrode is observed. The
506 presented voltammograms obtained from PyPP1/poly-Au electrodes (Fig.
507 4b) show that peak currents become smaller at faster electrolyte convection
508 rates. Smaller peak currents in case of shorter lifetime of thiolates in the
509 double layer region indicate a catalytic activity on the Au electrode through
510 the presence of desorbed thiolates. A similar behavior was observed with
511 PyPP1/Au(111) electrodes; the second H_2 -related peak became smaller com-
512 pared to the first desorption-related peak when the CVs were recorded with
513 a lower scan rate (comparing Fig. 2a and Fig. 3a). Altogether these observa-
514 tions indicate a diffusion-related phenomenon. The catalytic effect observed
515 for HER requires the presence PyPP1 monolayers on the electrode surface
516 without covalent bond to the electrode.

517 The above-stated arguments lead to models for the overall desorption

518 mechanism of the investigated thiols. First, consider the desorption of PyPP1.
 519 As shown in Reaction 1, thiol desorption requires exchange of electrons be-
 520 tween Au substrate and thiols. This reaction, however, involves also the
 521 substitution of thiol molecules with water on the Au surface [35],



524 Since Reaction 2 (where y stands for the number of water molecules required
 525 for the solvation of the thiolate) occurs at sufficiently negative potentials for
 526 HER, the adsorbed water layer is immediately consumed for formation of
 527 H_2 ,



530 Reactions 2 and 3 are reactions that occur for any type of thiol on an Au
 531 surface. It must be pointed out that the participation of HER in the desorp-
 532 tion process leads to an current contribution also, which may account for the
 533 fact that the integrated desorption currents are slightly higher than required
 534 for monolayer desorption. In this specific case, especially for desorption of
 535 PyPP1, the question arises: What is the reason of the temporary acceleration
 536 of Reaction 3? In the following, several possible models will be discussed.
 537 The overall model is schematically summarized in Fig. 6.

538 One possible reason for high HER rates associated with desorption is the
 539 retarded surface reconstruction of the Au substrate. It is currently widely
 540 accepted that thiolate bonding on Au results in a lower density of Au surface
 541 atoms compared to the SAM-free surface. SAM formation involves displace-
 542 ment of Au atoms on the surface; lifting the Herringbone reconstruction and
 543 formation of vacancy islands (etch pits). Recent studies demonstrated that

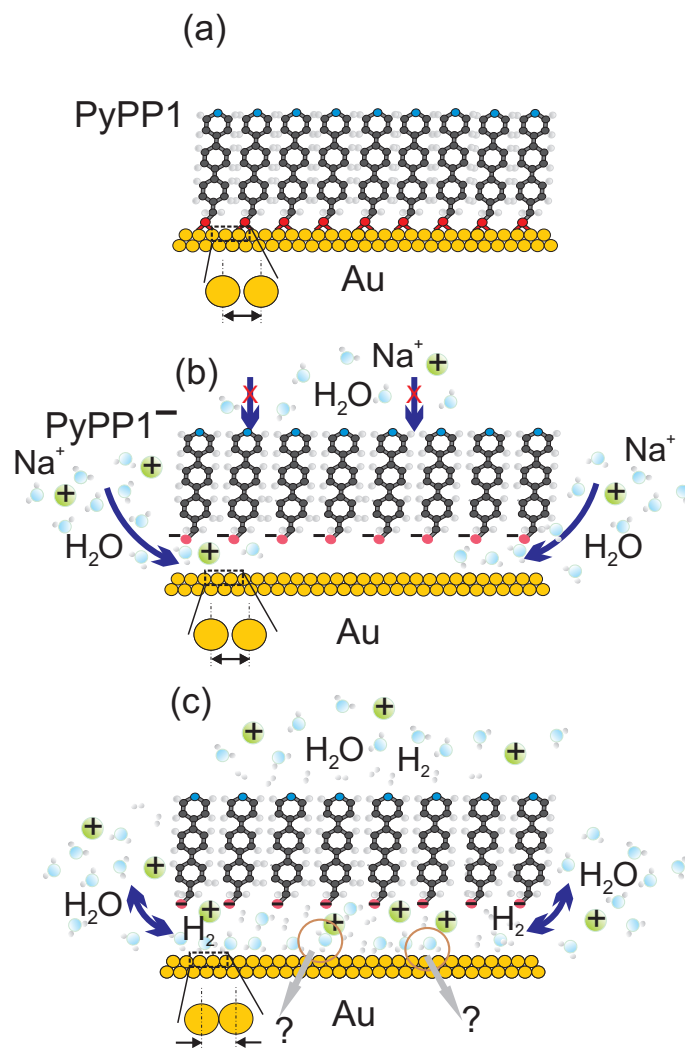


Figure 6: Schematic view of the proposed model for the rapid HER. (a) shows the intact SAM, which is reductively desorbed (b). Subsequent transport of water into the region between desorbed monolayer and Au leads to H₂ evolution (c).

544 together with vacancy islands, additional Au adatoms are formed, which serve
545 as energetically favoured bonding sites for thiolates [69–71]. Compared to a
546 reconstructed surface, such a modified Au surface underneath the SAM may
547 offer more catalytically active sites for reactions such as HER, if it becomes
548 accessible to the electrolyte. However, it has been reported for alkyl-thiols
549 that desorption of the SAM immediately initiates surface reconstruction, in-
550 cluding formation of the herringbone structure on Au(111), roughening of
551 step edges, formation of gold islands and disappearance of vacancy islands
552 [30, 72–74]. However, because the adsorption of the aliphatic and araliphatic
553 thiols result in the same changes on an Au surface [43, 57], a similar recon-
554 struction mechanism is expected for both thiol types after reductive desorp-
555 tion. For aliphatic thiols, no increase in the HER rate is, however, observed.
556 As a result, a substantial difference on the Au surface after reductive desorp-
557 tion of aliphatic and araliphatic SAMs is unlikely but cannot be completely
558 ruled out here.

559 Catalysis of HER through physical interactions between the Au surface
560 and any units of the desorbed thiolates, *e.g.*, the pyridine moiety, can be
561 safely ruled out as a possible explanation, due to the orientation of thiolates
562 in the related potential region. In this orientation, only the sulfur heads are
563 facing to the Au surface, separated from the Au surface by an electrolyte gap
564 of ~ 1 nm [75, 76]. Assuming a similar separation distance for PyPP1 thio-
565 lates, a strong influence of the ordered, suspended thiolates on the structure
566 of the electrolyte between Au and desorbed SAM is expected. In any assem-
567 bly form, the suspended negatively charged thiolates are prone to interactions
568 with counter ions in the solution. Protonation of electroreductively desorbed

569 *n*-alkanethiolates has been suggested despite the high solution *pH* [77, 78].
570 However, at *pH* 13, protonation of the full monolayer is not expected, as
571 the pK_a values for HS-R units are usually lower,[78] *e.g.* for $C_6H_5-CH_2-SH$,
572 $pK_a \sim 9.4$. [79]

573 The most likely mechanism for the observed acceleration of the HER after
574 reductive desorption of the thiol SAM involves orientation of water molecules
575 in the gap between Au and suspended monolayer. Diffusion of positively
576 charged counter ions, in this case $Na_{(aq)}^+$, from the electrolyte is essential
577 for desorption of SAMs [77]. If the desorbed thiulates form aggregates, a
578 homogenous charge distribution on the Au surface is quickly established.
579 On the other hand, if the organic layer does not lose its two-dimensional
580 order after desorption, as observed here, $Na_{(aq)}^+$ will be present in a hydrated
581 form between the negatively charged thiolate and the negatively polarized
582 Au surface (Fig. 6b). This additional layer of hydrated positive ions in the
583 gap between the organic layer and the Au surface is suggested here to lead
584 to an optimum pre-orientation of water for a participation in the HER, and
585 consequently higher HER rates (Fig. 6c). The ideal orientation of water
586 needed for participation in the HER is not known. Two possible candidates
587 are marked in Fig. 6c, though to achieve direct experimental evidence is
588 difficult.

589 The suggested model for the catalysis of HER — though speculative at
590 this point — can be employed to explain the double peaks observed on the
591 voltammograms upon desorption of the SAMs. For the catalytic activity
592 through water reorientation, transport of $Na_{(aq)}^+$ from bulk solution into the
593 gap between the thiolate monolayer and the Au surface is required. PyPP1

594 thiolates with orientation as observed are not prone to electrolyte penetra-
595 tion through the suspended film. Water and ion transport from the bulk
596 electrolyte into the volume between Au and suspended monolayer occurs
597 through inherent structural defects in the organic monolayer, such as do-
598 main boundaries. On an Au(111) surface, after consumption of the initially
599 adsorbed water layer, further water transport into the inner plane requires
600 additional time due to the existence of large electrolyte-blocking SAM do-
601 mains and a low amount of defects in the thiolate layer. Therefore, currents
602 from the catalyzed HER are seen in a peak that is separated from the thiol
603 reduction peak (Fig. 2a), and in general currents show a diffusion-related
604 behavior in the electrochemical experiments. On poly-Au, due to the higher
605 amount of structural defects in the SAM, electrochemical desorption and
606 subsequent transport of electrolyte into the gap occur much faster, so that
607 currents from both Faradaic reactions overlap (Fig. 2c). With increasing
608 amount of water molecules in the gap between the suspended thiolate layer
609 and the Au surface, contribution of HER to the peak currents increases. In
610 the proposed mechanism, depletion of thiolate molecules causes loss of the
611 observed catalytic activity, because the optimum distribution of $\text{Na}_{(\text{aq})}^+$ de-
612 pends on the existence of the oriented thiolates in the double layer. Because
613 the suspended thiolate layer also hinders the transport of the produced H_2
614 gas from the Au surface, the observed rate increase does not last long. In
615 addition to formation of macroscopic bubbles, which are observed at strongly
616 cathodic potentials only, the formed H_2 can be adsorbed either between Au
617 and suspended SAM, or at the SAM/electrolyte interface.

618 4. Conclusions

619 An accelerated (“rapid”) HER has been detected concurrent to desorp-
620 tion of structurally stable PyPP1 SAMs. The rate of the HER is strongly
621 influenced by the structure of desorbed thiolates residing near the electrode
622 surface after desorption. *In situ* ellipsometry results show a decrease of the
623 interfacial refractive index upon SAM desorption. Combined electrochemical
624 and SFG spectroscopy investigations show that after electroreductive desorp-
625 tion, the structural order of the araliphatic thiol films is inherited from the
626 chemisorbed state. For the compact PyPP1-SAM the two-dimensional or-
627 der is astonishingly stable. Comparison with the less compact PyPP2-SAM,
628 where two-dimensional order is not persevered upon reductive desorption, as
629 well as with literature data on aliphatic SAMs, shows that the structural sta-
630 bility of the desorbed SAM is a prerequisite for the occurrence of the increase
631 in HER rate.

632 The results imply that the presence of a highly ordered adsorbed layer of
633 non-redox active species can increase, rather than decrease, the rate of an
634 interfacial electron transfer reaction, in this case of the HER, here likely due
635 to the ordering effect of the organic monolayer on the solvent and reagent wa-
636 ter. The ordering effect occurs *via* the transient species of thiolates residing
637 in the double layer region immediately after cleavage of the Au-S bond. The
638 stability of the SAM after desorption is crucial for the observed effect. The
639 exact nature of the interfacial water requires detailed investigations from a
640 combination of vibrational spectroscopies and molecular simulations.

641 **Acknowledgement**

642 M.I.M. thanks the IMPRS SurMat for a scholarship. A. Terfort gener-
643 ously provided the substances for this study. M. Stratmann is acknowledged
644 for his continuous support. C.B. and P.K. acknowledge support from the
645 Helmholtz Program BioInterfaces and P.K. from NIH Grant EB-002027 to
646 the National ESCA and Surface Analysis Center for Biomedical Problems.
647 Y. C. thanks for support from the European Union and the state of North
648 Rhine-Westphalia in the frame of the HighTech.NRW program.

649 **References**

- 650 [1] S. B. Sachs, S. P. Dudek, R. P. Hsung, L. R. Sita, J. F. Smalley, M. D.
651 Newton, S. W. Feldberg, C. E. D. Chidsey, Rates of interfacial electron
652 transfer through π -conjugated spacers, *J. Am. Chem. Soc.* 119 (1997)
653 10563.
- 654 [2] D. M. Adams, L. Brus, C. E. D. Chidsey, S. Creager, C. Creutz, C. R.
655 Kagan, P. V. Kamat, M. Lieberman, S. Lindsay, R. A. Marcus, R. M.
656 Metzger, M. E. Michel-Beyerle, J. R. Miller, M. D. Newton, D. R. Rolis-
657 son, O. Sankey, K. S. Schanze, J. Yardley, X. Zhu, Charge transfer on
658 the nanoscale: current status, *J. Phys. Chem. B* 107 (2003) 6668.
- 659 [3] N. K. Chaki, K. Vijayamohanan, Self-assembled monolayers as a tunable
660 platform for biosensor applications, *Biosens. Bioelectron.* 17 (2002) 1.
- 661 [4] J. Gooding, F. Mearns, W. Yang, J. Liu, Self-assembled monolayers into
662 the 21st century: Recent advances and applications, *Electroanalysis* 15
663 (2003) 81.

- 664 [5] M. Frasconi, F. Mazzei, T. Ferri, Protein immobilization at goldthiol
665 surfaces and potential for biosensing, *Anal. Bioanal. Chem.* 398 (2010)
666 1545.
- 667 [6] T. Baunach, V. Ivanova, D. Kolb, H.-G. Boyen, P. Ziemann, M. Büttner,
668 P. Oelhafen, A new approach to the electrochemical metallization of
669 organic monolayers: Palladium deposition onto a 4,4-dithiodipyridine
670 self-assembled monolayer, *Adv. Mater.* 16 (2004) 2024.
- 671 [7] C. Silien, D. Lahaye, M. Caffio, R. Schaub, N. R. Champness,
672 M. Buck, Electrodeposition of palladium onto a pyridine-terminated
673 self-assembled monolayer, *Langmuir* 27 (2011) 2567.
- 674 [8] M. I. Muglali, J. Liu, A. Bashir, D. Borissov, M. Xu, Y. Wang, C. Woll,
675 M. Rohwerder, On the complexation kinetics for metallization of or-
676 ganic layers: palladium onto a pyridine-terminated araliphatic thiol film,
677 *Phys. Chem. Chem. Phys.* 14 (2012) 4703.
- 678 [9] M. Rohwerder, M. Stratmann, Surface modification by ordered mono-
679 layers: New ways of protecting materials against corrosion, *MRS Bull.*
680 24 (1999) 43.
- 681 [10] J. Mathiyarasu, S. Pathak, V. Yegnaraman, Review on corrosion pre-
682 vention of copper using ultrathin organic monolayers, *Corros. Rev.* 24
683 (2006) 281.
- 684 [11] F. Caprioli, F. Decker, A. G. Marrani, M. Beccari, V. D. Castro, Copper
685 protection by self-assembled monolayers of aromatic thiols in alkaline
686 solutions, *Phys. Chem. Chem. Phys.* 12 (2010) 9230.

- 687 [12] M. I. Muglali, A. Bashir, M. Rohwerder, A study on oxygen reduc-
688 tion inhibition at pyridine-terminated self assembled monolayer modified
689 Au(111) electrodes, *Phys. Status Solidi A* 207 (2010) 793.
- 690 [13] A. Nowicka, U. Hasse, G. Sievers, M. Donten, Z. Stojek, S. Fletcher,
691 F. Scholz, Selective knockout of gold active sites, *Angew. Chem., Int.*
692 *Ed.* 49 (2010) 3006.
- 693 [14] T. Uchida, H. Mogami, A. Yamakata, Y. Sasaki, M. Osawa, Hydro-
694 gen evolution reaction catalyzed by proton-coupled redox cycle of 4,4-
695 bipyridine monolayer adsorbed on silver electrodes, *J. Am. Chem. Soc.*
696 130 (2008) 10862.
- 697 [15] R. Alkire, D. Kolb, J. Lipkowski, P. Ross, *Chemically Modified Elec-*
698 *trodes*, Wiley-VCH, Weinheim, 2009.
- 699 [16] M. Rohwerder, K. de Weldige, M. Stratmann, Potential dependence of
700 the kinetics of thiol self-organization on Au(111), *J. Solid State Elec-*
701 *trochem.* 2 (1998) 88.
- 702 [17] F. Ma, R. B. Lennox, Potential-assisted deposition of alkanethiols on Au:
703 Controlled preparation of single- and mixed-component SAMs, *Lang-*
704 *muir* 16 (2000) 6188.
- 705 [18] M. J. Esplandiú, H. Hagenström, D. M. Kolb, Functionalized self-
706 assembled alkanethiol monolayers on Au(111) electrodes: 1. Surface
707 structure and electrochemistry, *Langmuir* 17 (2001) 828.
- 708 [19] N. Darwish, P. K. Eggers, S. Ciampi, Y. Zhang, Y. Tong, S. Ye, M. N.
709 Paddon-Row, J. J. Gooding, Reversible potential-induced structural

- 710 changes of alkanethiol monolayers on gold surfaces, *Electrochem. Com-*
711 *mun.* 13 (2011) 387.
- 712 [20] J. Zhang, A. C. Welinder, Q. Chi, J. Ulstrup, Electrochemically con-
713 trolled self-assembled monolayers characterized with molecular and sub-
714 molecular resolution, *Phys. Chem. Chem. Phys.* 13 (2011) 5526.
- 715 [21] W. Wang, S. Zhang, P. Chinwangso, R. C. Advincula, T. R. Lee, Electric
716 potential stability and ionic permeability of sams on gold derived from
717 bidentate and tridentate chelating alkanethiols, *J. Phys. Chem. C* 113
718 (2009) 3717.
- 719 [22] C. A. Widrig, C. Chung, M. D. Porter, The electrochemical desorption
720 of n-alkanethiol monolayers from polycrystalline Au and Ag electrodes,
721 *J. Electroanal. Chem. Interfacial Electrochem.* 310 (1991) 335.
- 722 [23] T. W. Schneider, D. A. Buttry, Electrochemical quartz crystal microbal-
723 ance studies of adsorption and desorption of self-assembled monolayers
724 of alkyl thiols on gold, *J. Am. Chem. Soc.* 115 (1993) 12391.
- 725 [24] P. Krysinski, R. V. Chamberlain, M. Majda, Partial electron transfer
726 in octadecanethiol binding to gold, *Langmuir* 10 (1994) 4286.
- 727 [25] D.-F. Yang, C. P. Wilde, M. Morin, Electrochemical desorption and
728 adsorption of nonyl mercaptan at gold single crystal electrode surfaces,
729 *Langmuir* 12 (1996) 6570.
- 730 [26] D. Hobar, K. Miyake, S.-I. Imabayashi, K. Niki, T. Kakiuchi, In-
731 situ scanning tunneling microscopy imaging of the reductive desorption
732 process of alkanethiols on Au(111), *Langmuir* 14 (1998) 3590.

- 733 [27] M. Byloos, H. Al-Maznai, M. Morin, Formation of a self-assembled
734 monolayer via the electrospreading of physisorbed micelles of thiolates,
735 J. Phys. Chem. B 103 (1999) 6554.
- 736 [28] A. Badía, Asymptotic theory for the inverse problem in magnetic force
737 microscopy of superconductors, Phys. Rev. B 60 (1999) 10436.
- 738 [29] S.-S. Wong, M. D. Porter, Origin of the multiple voltammetric des-
739 orption waves of long-chain alkanethiolate monolayers chemisorbed on
740 annealed gold electrodes, J. Electroanal. Chem. 485 (2000) 135.
- 741 [30] H. Wano, K. Uosaki, In situ, real-time monitoring of the reductive des-
742 orption process of self-assembled monolayers of hexanethiol on Au(111)
743 surfaces in acidic and alkaline aqueous solutions by scanning tunneling
744 microscopy, Langmuir 17 (2001) 8224.
- 745 [31] C. Vericat, G. Andreassen, M. E. Vela, H. Martin, R. C. Salvarezza,
746 Following transformation in self-assembled alkanethiol monolayers on
747 Au(111) by in situ scanning tunneling microscopy, J. Chem. Phys. 115
748 (2001) 6672.
- 749 [32] Y.-T. Long, H.-T. Rong, M. Buck, M. Grunze, Odd-even effects in
750 the cyclic voltammetry of self-assembled monolayers of biphenyl based
751 thiols, J. Electroanal. Chem. 524 (2002) 62.
- 752 [33] T. Kakiuchi, H. Usui, D. Hobarra, M. Yamamoto, Voltammetric proper-
753 ties of the reductive desorption of alkanethiol self-assembled monolayers
754 from a metal surface, Langmuir 18 (2002) 5231.

- 755 [34] I. Thom, M. Buck, Electrochemical stability of self-assembled monolay-
756 ers of biphenyl based thiols studied by cyclic voltammetry and second
757 harmonic generation, *Surf. Sci.* 581 (2005) 33.
- 758 [35] T. Laredo, J. Leitch, M. Chen, I. J. Burgess, J. R. Dutcher, J. Lipkowski,
759 Measurement of the charge number per adsorbed molecule and packing
760 densities of self-assembled long-chain monolayers of thiols, *Langmuir* 23
761 (2007) 6205.
- 762 [36] R. Aguilar-Sanchez, G. J. Su, M. Homberger, U. Simon, T. Wand-
763 lowski, Structure and electrochemical characterization of 4-methyl-4-
764 (n-mercaptoalkyl)biphenyls on Au(111)-(1×1), *J. Phys. Chem. C* 111
765 (2007) 17409.
- 766 [37] I. Thom, M. Buck, On the interpretation of multiple waves in cyclic
767 voltammograms of self-assembled monolayers of n-alkane thiols on gold,
768 *Z. Phys. Chem.* 222 (2008) 739.
- 769 [38] X. Cai, S. Baldelli, Surface barrier properties of self-assembled mono-
770 layers as deduced by sum frequency generation spectroscopy and elec-
771 trochemistry, *J. Phys. Chem. C* 115 (2011) 19178.
- 772 [39] C. Humbert, B. Busson, C. Six, A. Gayral, M. Gruselle, F. Villain,
773 A. Tadjeddine, Sum-frequency generation as a vibrational and electronic
774 probe of the electrochemical interface and thin films, *J. Electroanal.*
775 *Chem.* 621 (2008) 314.
- 776 [40] H. Zhang, S. Baldelli, Alkanethiol monolayers at reduced and oxidized

- 777 zinc surfaces with corrosion protection: a sum frequency generation and
778 electrochemistry investigation, *J. Phys. Chem. B* 110 (2006) 24062.
- 779 [41] H. Zhang, C. Romero, S. Baldelli, Preparation of alkanethiol monolay-
780 ers on mild steel surfaces studied with sum frequency generation and
781 electrochemistry, *J. Phys. Chem. B* 109 (2005) 15520.
- 782 [42] Y. Zhang, Y. Tong, M. Abe, K. Uosaki, M. Osawa, Y. Sasaki, S. Ye, Fab-
783 rication of photochemical pattern on a self-assembled monolayer (SAM)
784 of a ruthenium cluster under electrochemical control, *J. Mater. Chem.*
785 19 (2009) 261.
- 786 [43] W. Azzam, A. Bashir, A. Terfort, T. Strunskus, C. Wöll, Combined
787 STM and FTIR characterization of terphenylalkanethiol monolayers on
788 Au(111): Effect of alkyl chain length and deposition temperature, *Lang-*
789 *muir* 22 (2006) 3647.
- 790 [44] Z. J. Donhauser, B. A. Mantooth, K. F. Kelly, L. A. Bumm, J. D.
791 Monnell, J. J. Stapleton, D. W. Price, A. M. Rawlett, D. L. Allara,
792 J. M. Tour, P. S. Weiss, Conductance switching in single molecules
793 through conformational changes, *Science* 292 (2001) 2303.
- 794 [45] D. I. Gittins, D. Bethell, D. J. Schiffrin, R. J. Nichols, A nanometre-scale
795 electronic switch consisting of a metal cluster and redox-addressable
796 groups, *Nature* 408 (2000) 67.
- 797 [46] M. I. Muglali, A. Bashir, A. Terfort, M. Rohwerder, Electrochemi-
798 cal investigations on stability and protonation behavior of pyridine-

- 799 terminated aromatic self-assembled monolayers, *Phys. Chem. Chem.*
800 *Phys.* 13 (2011) 15530.
- 801 [47] B. Schupbach, A. Terfort, A divergent synthesis of oligoarylalkanethiols
802 with lewis-basic n-donor termini, *Org. Biomol. Chem.* 8 (2010) 3552.
- 803 [48] Y. Chen, P. Schneider, A. Erbe, Investigation of native oxide growth
804 on zinc in different atmospheres by spectroscopic ellipsometry, *Phys.*
805 *Status Solidi A* 209 (2012) 846.
- 806 [49] Y. Chen, A. Erbe, In situ spectroscopic ellipsometry during electro-
807 chemical treatment of zinc in alkaline carbonate electrolyte, *Surf. Sci.*
808 607 (2013) 39.
- 809 [50] R. M. A. Azzam, N. M. Bashara, *Ellipsometry and Polarized Light*,
810 Elsevier Science, Amsterdam, 1999.
- 811 [51] J. Lekner, *Theory of Reflection of Electromagnetic and Particle Waves*,
812 M. Nijhoff, Dordrecht, 1987.
- 813 [52] D. R. Lide (Ed.), *Handbook of Chemistry and Physics*, CRC Press, Boca
814 Raton, 90th edition, 2009.
- 815 [53] P. G. Etchegoin, E. C. Le Ru, M. Meyer, An analytic model for the
816 optical properties of gold, *J. Chem. Phys.* 125 (2006) 164705.
- 817 [54] P. G. Etchegoin, E. C. L. Ru, M. Meyer, Erratum: "An analytic model
818 for the optical properties of gold" [*J. Chem. Phys.*, 164705 (2006)], *J.*
819 *Chem. Phys.* 127 (2007) 189901.

- 820 [55] D. Verreault, V. Kurz, C. Howell, P. Koelsch, Sample cells for probing
821 solid/liquid interfaces with broadband sum-frequency-generation spec-
822 troscopy, *Rev. Sci. Instrum.* 81 (2010) 063111.
- 823 [56] A. Lagutchev, S. A. Hambir, D. D. Dlott, Nonresonant background
824 suppression in broadband vibrational sum-frequency generation spec-
825 troscopy, *J. Phys. Chem. C* 111 (2007) 13645.
- 826 [57] J. Liu, B. Schupbach, A. Bashir, O. Shekhah, A. Nefedov, M. Kind,
827 A. Terfort, C. Wöll, Structural characterization of self-assembled mono-
828 layers of pyridine-terminated thiolates on gold, *Phys. Chem. Chem.*
829 *Phys.* 12 (2010) 4459.
- 830 [58] D.-F. Yang, M. Morin, Chronoamperometric study of the reduction of
831 chemisorbed thiols on Au(111), *J. Electroanal. Chem.* 429 (1997) 1.
- 832 [59] D.-F. Yang, M. Morin, Chronoamperometric study of the reductive des-
833 orption of alkanethiol self-assembled monolayers, *J. Electroanal. Chem.*
834 441 (1998) 173.
- 835 [60] K. Arihara, T. Ariga, N. Takashima, K. Arihara, T. Okajima, F. Ki-
836 tamura, K. Tokuda, T. Ohsaka, Multiple voltammetric waves for re-
837 ductive desorption of cysteine and 4-mercaptobenzoic acid monolayers
838 self-assembled on gold substrates, *Phys. Chem. Chem. Phys.* 5 (2003)
839 3758.
- 840 [61] M. S. El-Deab, K. Arihara, T. Ohsaka, Fabrication of Au(111)-like poly-
841 crystalline gold electrodes and their applications to oxygen reduction,
842 *J. Electrochem. Soc.* 151 (2004) E213.

- 843 [62] R. Madueño, J. Sevilla, T. Pineda, A. Román, M. Blázquez, A voltam-
844 metric study of 6-mercaptopurine monolayers on polycrystalline gold
845 electrodes, *J. Electroanal. Chem.* 506 (2001) 92.
- 846 [63] J. Strutwolf, C. O’Sullivan, Microstructures by selective desorption of
847 self-assembled monolayer from polycrystalline gold electrodes, *Electro-*
848 *analysis* 19 (2007) 1467.
- 849 [64] T. Kondo, T. Sumi, K. Uosaki, A rotating gold ring-gold disk electrode
850 study on electrochemical reductive desorption and oxidative readsorp-
851 tion of a self-assembled monolayer of dodecanethiol, *J. Electroanal.*
852 *Chem.* 538 (2002) 59.
- 853 [65] P. Koelsch, M. Muglali, M. Rohwerder, A. Erbe, Third-order effects
854 in resonant sum-frequency-generation signals at electrified metal/liquid
855 interfaces, *J. Opt. Soc. Am. B* accepted (2012).
- 856 [66] D.-F. Yang, H. Al-Maznai, M. Morin, Vibrational study of the fast
857 reductive and the slow oxidative desorptions of a nonanethiol self-
858 assembled monolayer from a Au(111) single crystal electrode, *J. Phys.*
859 *Chem. B* 101 (1997) 1158.
- 860 [67] M. Esplandiu, M. Carot, F. Cometto, V. Macagno, E. Patrito,
861 Electrochemical STM investigation of 1,8-octanedithiol monolayers on
862 Au(111): Experimental and theoretical study, *Surf. Sci.* 600 (2006) 155.
- 863 [68] J. N. Israelachvili, *Intermolecular and Surface Forces*, Academic Press,
864 London, 1992.

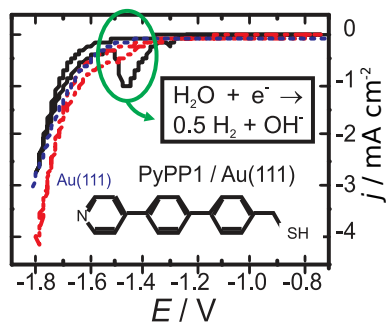
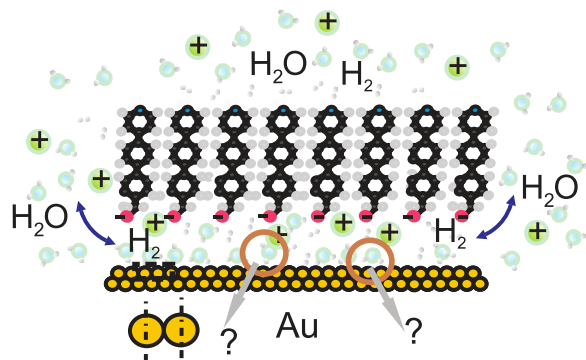
- 865 [69] E. Torres, P. U. Biedermann, A. T. Blumenau, The role of gold adatoms
866 in self-assembled monolayers of thiol on Au(111), *Int. J. Quantum*
867 *Chem.* 109 (2009) 3466.
- 868 [70] D. P. Woodruff, The interface structure of n-alkylthiolate self-assembled
869 monolayers on coinage metal surfaces, *Phys. Chem. Chem. Phys.* 10
870 (2008) 7211.
- 871 [71] H. Hakkinen, The gold-sulfur interface at the nanoscale, *Nat. Chem.* 4
872 (2012) 443.
- 873 [72] H. Wano, K. Uosaki, In situ dynamic monitoring of electrochemical ox-
874 idative adsorption and reductive desorption processes of a self-assembled
875 monolayer of hexanethiol on a Au(111) surface in KOH ethanol solution
876 by scanning tunneling microscopy, *Langmuir* 21 (2005) 4024.
- 877 [73] D. Hobara, M. Yamamoto, T. Kakiuchi, Reconstruction of Au(111)
878 following the reductive desorption of self-assembled monolayers of 2-
879 mercaptoethanesulfonic acid studied by in situ scanning tunneling mi-
880 croscopy, *Chem. Lett.* 30 (2001) 374.
- 881 [74] D. Hobara, M. Yamamoto, T. Kakiuchi, Reconstruction of Au(111)
882 following the reductive desorption of self-assembled monolayers of 2-
883 mercaptoethanesulfonic acid studied by in situ scanning tunneling mi-
884 croscopy (pg 375, 2001), *Chem. Lett.* 30 (2001) 1200.
- 885 [75] I. Burgess, V. Zamlynny, G. Szymanski, A. Schwan, R. Faragher, J. Lip-
886 kowski, J. Majewski, S. Satija, Neutron reflectivity studies of field driven

- 887 transformations in a monolayer of 4-pentadecyl pyridine at Au electrode
888 surfaces, *J. Electroanal. Chem.* 550 (2003) 187.
- 889 [76] I. Burgess, M. Li, S. Horswell, G. Szymanski, J. Lipkowski, J. Majewski,
890 S. Satija, Electric field-driven transformations of a supported model
891 biological membrane - an electrochemical and neutron reflectivity study,
892 *Biophys. J.* 86 (2004) 1763.
- 893 [77] D.-F. Yang, C. P. Wilde, M. Morin, Studies of the electrochemical
894 removal and efficient re-formation of a monolayer of hexadecanethiol self-
895 assembled at an Au(111) single crystal in aqueous solutions, *Langmuir*
896 13 (1997) 243.
- 897 [78] M. Byloos, S. Rifai, H. Al-Maznai, M. Laferrière, M. Morin, A second
898 harmonic generation study of a physisorbed precursor to the electrode-
899 position of a monolayer of alkanethiols, *Langmuir* 17 (2001) 2478.
- 900 [79] M. M. Kreevoy, E. T. Harper, R. E. Duvall, H. S. Wilgus, L. T. Ditsch,
901 Inductive effects on the acid dissociation constants of mercaptans, *J.*
902 *Am. Chem. Soc.* 82 (1960) 4899.

903 **Highlights**

- 904 • Aliphatic SAM with extraordinary electrochemical stability
- 905 • Enhancement of the hydrogen evolution after reductive SAM desorp-
906 tion
- 907 • In situ real time sum frequency generation spectroscopy (SFG)
- 908 • Relation between reductive SAM desorption and hydrogen evolution

909 Graphical abstract



910